A geometric perspective: experimental evaluation of the quantum Cramér-Rao bound

Changhao Li (李长昊),[1,2] Mo Chen (陈墨),[1,3,4] and Paola Cappellaro[1,2,5,*]

[1]*Research Laboratory of Electronics, Massachusetts Institute of Technology, Cambridge, Massachusetts 02139, USA*
[2]*Department of Nuclear Science and Engineering,*
Massachusetts Institute of Technology, Cambridge, Massachusetts 02139, USA
[3]*Institute for Quantum Information and Matter,*
California Institute of Technology, Pasadena, CA 91125, USA
[4]*Thomas J. Watson, Sr., Laboratory of Applied Physics,*
California Institute of Technology, Pasadena, CA 91125, USA
[5]*Department of Physics, Massachusetts Institute of Technology, Cambridge, Massachusetts 02139, USA*

The power of quantum sensing rests on its ultimate precision limit, quantified by the quantum Cramér-Rao bound (QCRB), which can surpass classical bounds. In multi-parameter estimation, the QCRB is not always saturated as the quantum nature of associated observables may lead to their incompatibility. Here we explore the precision limits of multi-parameter estimation through the lens of quantum geometry, enabling us to experimentally evaluate the QCRB via quantum geometry measurements. Focusing on two- and three-parameter estimation, we elucidate how fundamental quantum uncertainty principles prevent the saturation of the bound. By linking a metric of "quantumness" to the system geometric properties, we investigate and experimentally extract the attainable QCRB for three-parameter estimations.

Quantum sensing stands as a key application for quantum technologies [1]. Quantum sensors promise to achieve better sensitivity or precision than classical systems and have been utilized in many fields, ranging from material science [2–6] to biology [7–10]. Quantum metrology quantifies the precision limit of quantum sensing with the quantum Cramér-Rao bound (QCRB) [11–17]. For unbiased estimation of an unknown system parameter, the QCRB is given by the inverse of the quantum Fisher information [14–17]. The estimator is chosen to be optimal, therefore the QCRB only depends on the quantum state. In turn, the precision of estimating a parameter can be linked to the "distance" between two nearby states differing by an infinitesimally small parameter change [16, 18–20]. This naturally connects quantum sensing to the quantum geometric properties of the system, as the quantum metric tensor is closely related to the ultimate estimation precision quantified by the quantum Fisher information.

This picture becomes more involved when extending the goal from estimating a single parameter to multiple parameters, in analogy to the complexity of multi-dimensional system versus 1D systems. The complication arises from the incompatibility between each parameter's optimal estimators–a signature of quantum mechanics [16, 17, 19]. This leads to trade-offs among the estimation precisions of different parameters when picking the initial state. This interplay among parameters makes the multi-parameter estimation problem more intriguing than single parameter estimation. Hence developing tools to investigate the ultimate precision and the attainable QCRB in a multi-parameter estimation setting is of great interest for quantum metrology and sensing applications. A promising strategy, similar to the single-parameter scenario, is to link quantum geometric properties of the (multi-)parametrized state to the estimation precision. Specifically, in addition to the link between the quantum metric tensor and the quantum Fisher information, we can link the non-commutativity of optimal measurement operators for different parameters to the Uhlmann curvature [15–17], as we explain below. Characterizing the geometry of the parametrized quantum states by measuring the quantum geometric tensor would thus help explore the problem of quantum multi-parameter estimation and evaluate the attainable QCRB from a geometric perspective.

In this work, we explore the relation between quantum geometry and multi-parameter estimation to gain novel insight into the corresponding precision bound. In particular, we show that geometric and parameter estimation metrics are connected via the *characterization number* γ, which characterizes the "quantumness" of the system. We find that the characterization number γ is linked to both metrology and geometry: γ is upper-bounded by the fundamental uncertainty relation and it can be a signature of exotic magnetic monopoles in parameter space. Beyond its theoretical insight, this relation provides a strategy to experimentally evaluate quantum estimation bounds. We can thus provide an experimental demonstration of these results by focusing on a three-parameter, three-level pure state model, which is synthesized using a single nitrogen-vacancy (NV) center in diamond. Based on measuring spin-1 Rabi oscillations upon parameter-modulated driving, we develop experimental tools to extract the geometric quantities and determine the quantum Fisher information and Uhlmann curvature of the quantum state. Then the system's quantumness, i.e., the incompatibility among parameters to be estimated, is characterized with the help of the characterization number γ. We finally evaluate the attainable QCRB for the

parameterized state, as well as the two-parameter states in the subspace of the three-parameter model.

Relating quantum geometry to quantum multi-parameter sensing We consider a generic quantum multi-parameter estimation problem given by a quantum statistic model $\rho_{\boldsymbol{\theta}}$, a family of density operator labelled by $\boldsymbol{\theta} = (\theta_1, \theta_2, ..., \theta_d)^T$ that is the set of unknown parameters to be estimated. Performing POVM $\mathcal{M} = \{\mathcal{M}_k | \sum_k \mathcal{M}_k = I, \mathcal{M}_k \geq 0\}$, we obtain the measurement conditional probabilities $p(k|\boldsymbol{\theta}) = \mathrm{Tr}[\rho_{\boldsymbol{\theta}}\mathcal{M}_k]$. With N repeated measurements, the unknown parameters are estimated via the estimator $\tilde{\boldsymbol{\theta}}(k)$. The accuracy of the estimation is quantified by the mean-square error matrix $\boldsymbol{V}(\boldsymbol{\theta}) = \sum_k p(k|\boldsymbol{\theta})[\tilde{\boldsymbol{\theta}}(k) - \boldsymbol{\theta}][\tilde{\boldsymbol{\theta}}(k) - \boldsymbol{\theta}]^T$. Obtaining the lower bounds of this error matrix is of critical importance in quantum sensing and metrology.

The bounds usually depend on the choice of POVM. The symmetric logarithmic derivative [11–13] (SLD) can be used to define a bound that only depends on the quantum statistic model $\rho_{\boldsymbol{\theta}}$, having optimized over the measurement operators. The SLD L_μ ($\mu \in \boldsymbol{\theta}$) is implicitly defined via the equation

$$\partial_\mu \rho_{\boldsymbol{\theta}} = \frac{L_\mu \rho_{\boldsymbol{\theta}} + \rho_{\boldsymbol{\theta}} L_\mu}{2}. \tag{1}$$

The corresponding quantum Fisher information matrix (QFIM), $\boldsymbol{J}(\boldsymbol{\theta})$, is given by

$$J_{\mu\nu}(\boldsymbol{\theta}) = \mathrm{Tr}[\rho_{\boldsymbol{\theta}} \frac{L_\mu L_\nu + L_\nu L_\mu}{2}], \tag{2}$$

which yields the matrix SLD QCRB $\boldsymbol{V}(\boldsymbol{\theta}) \geq \boldsymbol{J}(\boldsymbol{\theta})^{-1}$. It is convenient to introduce a scalar QCRB, $C^S(\boldsymbol{\theta}, \boldsymbol{W}) = \mathrm{Tr}\left[\boldsymbol{W}\boldsymbol{J}(\boldsymbol{\theta})^{-1}\right]$. For a weight matrix $\boldsymbol{W}$, the inequality becomes $\mathrm{Tr}\left[\boldsymbol{W}\boldsymbol{V}\right] \geq C^S(\boldsymbol{\theta}, \boldsymbol{W})$. This SLD-CRB is generally not attainable due to the incompatibility of generators of different parameters. That is, the optimal measurement operators corresponding to different parameters do not commute with each other, making this scalar bound unreachable.

Holevo derived [14] a tighter scalar bound, the Holevo Cramér-Rao bound (HCRB) $C^H(\boldsymbol{\theta}, \boldsymbol{W})$, which is however only obtained as an optimization. More recently, it has been shown that these two scalar bounds satisfy the following inequality [15]

$$\begin{aligned} C^S(\boldsymbol{\theta}, \boldsymbol{W}) &\leq C^H(\boldsymbol{\theta}, \boldsymbol{W}) \\ &\leq C^S(\boldsymbol{\theta}, \boldsymbol{W}) + ||\sqrt{\boldsymbol{W}}\boldsymbol{J}^{-1}\boldsymbol{F}\boldsymbol{J}^{-1}\sqrt{\boldsymbol{W}}||_1 \\ &\leq (1+\gamma)C^S(\boldsymbol{\theta}, \boldsymbol{W}) \leq 2C^S(\boldsymbol{\theta}, \boldsymbol{W}), \end{aligned} \tag{3}$$

where $|| \cdot ||_1$ denotes the trace norm and $\boldsymbol{F}$ is known as the mean Uhlmann curvature with element $F_{\mu\nu} = -\frac{i}{4}\mathrm{Tr}[\rho_{\boldsymbol{\theta}}[L_\mu, L_\nu]]$ (for pure states this reduces to the Berry curvature.) The *characterization number* γ that appears in Eq. (3) is defined as

$$\gamma = ||i2\boldsymbol{J}^{-1}\boldsymbol{F}||_\infty, \tag{4}$$
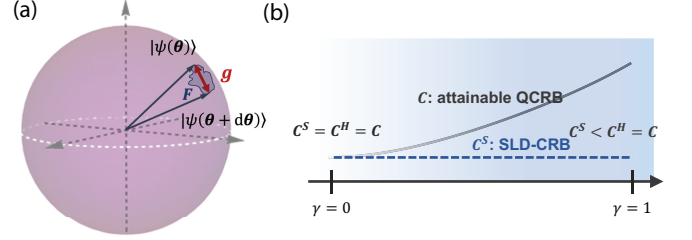
FIG. 1. **(a).** Diagram showing the "distance" between nearby states $|\psi(\boldsymbol{\theta})\rangle$ and $|\psi(\boldsymbol{\theta} + d\boldsymbol{\theta})\rangle$ in parameter space, from which the metric tensor $\boldsymbol{g}$ (proportional to quantum Fisher information $\boldsymbol{J}$) and Berry curvature $\boldsymbol{F}$ naturally arise. **(b).** SLD-CRB and attaianable QCRB for different γ values. At $\gamma = 0$ the model is quasi-classical and the SLD-CRB is reachable, i.e., $C^S = C^H = C$, while the model is called coherent at $\gamma = 1$ with $C^S < C^H = C$. Here we take the weight matrix $\boldsymbol{W} = \boldsymbol{J}$ and denote $C^{S(H)}(\boldsymbol{\theta}, \boldsymbol{W})$ as $C^{S(H)}$ for simplicity.

where $||\boldsymbol{A}||_\infty$ denotes the largest eigenvalue of $\boldsymbol{A}$. γ characterizes the "quantumness" of the system, i.e., it quantifies the amount of incompatibility of the statistic model $\rho_{\boldsymbol{\theta}}$. As implicit in Eq. (3) and explained hereafter, it can be proved that $0 \leq \gamma \leq 1$ [15].

An explicit expression for an attainable scalar QCRB with weight matrix $\boldsymbol{W} = \boldsymbol{J}$, which monotonically increases with γ, was derived in Ref. [21, 22]

$$\begin{aligned} C(\boldsymbol{\theta}) &= \mathrm{Tr}\left[\mathrm{Re}\left[\sqrt{\mathbb{1}_d + 2i\boldsymbol{J}(\boldsymbol{\theta})^{-1/2}\boldsymbol{F}(\boldsymbol{\theta})\boldsymbol{J}(\boldsymbol{\theta})^{-1/2}}\right]^{-2}\right] \\ &= \sum_i \frac{2}{1 + \sqrt{1 - |\gamma_i|^2}}, \end{aligned} \tag{5}$$

where $\mathbb{1}_d$ is the d-dimensional identity matrix and γ_i is the i-th eigenvalue of $i2\boldsymbol{J}^{-1}\boldsymbol{F}$. The evaluation of this *attainable QCRB* in terms of geometric quantities, and its relation with SLD-CRB and HCRB, is our key result.

To highlight the geometric interpretation of $\boldsymbol{J}, \boldsymbol{F}$ (so-far introduced via the SLD) and thus the connection between estimation and geometry, in the following we consider pure state models, i.e., $\rho_{\boldsymbol{\theta}} = |\psi(\boldsymbol{\theta})\rangle\langle\psi(\boldsymbol{\theta})|$. The geometric properties of this state are captured by the quantum geometric tensor (QGT), which naturally appears when one considers the "distance" between nearby states $|\psi(\boldsymbol{\theta})\rangle$ and $|\psi(\boldsymbol{\theta} + d\boldsymbol{\theta})\rangle$ (Fig. 1):

$$ds^2 \equiv 1 - |\langle\psi(\boldsymbol{\theta})|\psi(\boldsymbol{\theta}) + d\boldsymbol{\theta}\rangle|^2 = d\theta_\mu \chi_{\mu\nu} d\theta_\nu + O(|d\boldsymbol{\theta}|^3).$$

Here we defined the QGT, given by $\chi_{\mu\nu} = \langle\partial_\mu\psi|(I - |\psi\rangle\langle\psi|)|\partial_\nu\psi\rangle = g_{\mu\nu} + \frac{i}{2}F_{\mu\nu}$. Its imaginary (antisymmetric) part $F_{\mu\nu}$ is the Berry curvature. The symmetric real part $g_{\mu\nu}$, also known as Fubini-Study metric tensor, characterizes the overlap between the nearby states. A larger $g_{\mu\nu}$ indicates a larger distinguishability between two states differing by an infinitesimal change of parameters, and it is thus related to a larger quantum Fisher

information. The role of the Berry curvature is subtler, as it links the attainability of the QFI bound in multi-parameter scenarios to the observable compatibility.

To show the relation between QGT and parameter estimation, one can assume the parameter $\boldsymbol{\theta}$ to be introduced by evolving an initial state $|\psi_0\rangle$ via a unitary evolution, i.e., $|\psi(\boldsymbol{\theta})\rangle = U(\boldsymbol{\theta})|\psi_0\rangle$. Then, the generator for parameter $\mu \in \boldsymbol{\theta}$ is the operator $\mathcal{G}_\mu \equiv i(\partial_\mu U)U^\dagger$. It can be shown that the QFIM $J_{\mu\nu}$ and the metric tensor $g_{\mu\nu}$ are related by [23]

$$J_{\mu\mu} = 4\left\langle \Delta\mathcal{G}_\mu^2 \right\rangle = 4g_{\mu\mu}, \quad J_{\mu\nu} = 4\mathrm{Cov}(\mathcal{G}_\mu, \mathcal{G}_\nu) = 4g_{\mu\nu}, \quad (6)$$

where $\left\langle \Delta\mathcal{G}_\mu^2 \right\rangle$ is the generator variance and $\mathrm{Cov}(\mathcal{G}_\mu, \mathcal{G}_\nu)$ their covariance. Similarly, the Berry curvature is given by the commutator between the parameter generators

$$F_{\mu\nu} = i\left\langle [\mathcal{G}_\mu, \mathcal{G}_\nu] \right\rangle. \quad (7)$$

It is now clear that the Berry curvature matrix characterizes the incompatibility of the system as it arises from the non-commutativity between generators of different parameters. When $F_{\mu\nu} = 0$ ($\forall\mu,\nu \in \boldsymbol{\theta}$), the characterization number is $\gamma = 0$ according to Eq. 4 and the system is quasi-classical. The discrepancy between the attainable QCRB and the SLD-CRB now vanishes, i.e., $C(\boldsymbol{\theta}) = C^S(\boldsymbol{\theta}, \boldsymbol{J}) = C^H(\boldsymbol{\theta}, \boldsymbol{J}) = \mathrm{Tr}[\mathbb{1}_d] = d$.

As one of the main contributions of this letter, we next show that in the opposite limit the characterization number γ is upper-bounded by the fundamental quantum uncertainty principles. We consider the two-parameter case and start from the Robertson-Schrödinger uncertainty relation for two operators $\hat{A}, \hat{B}$ [24], which is the stronger version of the better-known Heisenberg uncertainty relation. In the quantum parameter estimation case, the operators $\hat{A}, \hat{B}$ can be replaced by the generators of parameters μ, ν, giving

$$\begin{aligned} \left\langle \Delta\mathcal{G}_\mu^2 \right\rangle \left\langle \Delta\mathcal{G}_\nu^2 \right\rangle &\geq \frac{1}{4}|\langle [\mathcal{G}_\mu, \mathcal{G}_\nu]\rangle|^2 + \frac{1}{4}\langle\{\mathcal{G}_\mu, \mathcal{G}_\nu\}\rangle^2 \\ &= \frac{1}{4}|\langle [\mathcal{G}_\mu, \mathcal{G}_\nu]\rangle|^2 + \mathrm{Cov}(\mathcal{G}_\mu, \mathcal{G}_\nu)^2. \end{aligned} \quad (8)$$

With Eq. (4,6,7) we have

$$\gamma = 2\frac{F_{\mu\nu}}{\sqrt{\det(\boldsymbol{J})}} = \frac{1}{2}\frac{F_{\mu\nu}}{\sqrt{\det(\boldsymbol{g})}} \leq 1, \quad (9)$$

which relates γ to half the Berry's phase along the curve that encloses a unit area induced by metric tensor. This relation holds for any two-parameter space in a multi-parameter setting. The above relation can also be derived from the fact that the QGT $\chi_{\mu\nu}$ is a positive semi-definite matrix and has been explored in various models [25–27]. Reversely, generalization of the two-operator product uncertainty relations Eq. 8 to multi-operators can be performed using the fact that $\gamma \leq 1$, as we show in the supplementary material [23].

As a concrete example, we consider a two-parameter model in a qubit system $|\psi(\theta,\phi)\rangle = \cos\left(\frac{\theta}{2}\right)|0\rangle - \sin\left(\frac{\theta}{2}\right)e^{-i\phi}|1\rangle$. The QFIM and Berry curvature matrix,

$$\boldsymbol{J} = \begin{pmatrix} 1 & 0 \\ 0 & \sin^2\theta \end{pmatrix}, \quad \boldsymbol{F} = \begin{pmatrix} 0 & \sin\theta/2 \\ -\sin\theta/2 & 0 \end{pmatrix}, \quad (10)$$

yield $\gamma = 1$, implying that the model is coherent and the two parameters θ,ϕ here are informationally exclusive. Indeed, they are associated with the non-commuting generators σ_z and σ_y, respectively.

Eq. (6-7) show the connection between quantum geometry and quantum multi-parameter estimation (Fig. 1). The value of γ characterizes both the quantum multi-parameter estimation scenario, where it is a measure of system's incompatibility, and the geometry of the quantum state manifold, where it relates the metric tensor determinant to the Berry curvature. This ratio is deeply connected to the existence of topological invariants. Indeed, more generally γ can be expressed as the ratio between an $n-$form generalized Berry curvature $F_{\alpha\beta...}$ and the determinant of the metric tensor, $\gamma = c\frac{F_{\alpha\beta...}}{\sqrt{det(\boldsymbol{g})}}$ with c being a constant normalization factor. Accordingly, γ is gauge-invariant and for pointlike or extended monopoles [28, 29], we have $\gamma(\boldsymbol{\theta}) = 1$, $\forall\boldsymbol{\theta}$ in parameter space, indicating the largest quantumness of these monopoles. The isotropy of γ is due to the radial nature of the field emanating from monopole sources; when $\gamma = 1$, the flux (i.e., the generalized Berry curvature) through an unit area (given by the metric tensor determinant) is unit and thus the flux integral over a closed sphere S^n gives the quantized topological number, upon normalization.

As an example, the previous two-parameter, qubit model $|\psi(\theta,\phi)\rangle$ describes pure states on a S^2 sphere such that the integral of their Berry curvature $F_{\mu\nu}$ over the sphere yields the first Chern number, corresponding to a Dirac monopole at the origin of parameter space.

In the following, we experimentally explore the relation between quantum geometry and quantum multi-parameter estimation. In particular, we measure the geometric quantities using a three-level system and demonstrate the relation (3) and obtain the attainable QCRB. By embedding a two-parameter model into a 3-level system, we can further explore scenarios away from the two bounds $\gamma = 0, 1$.

Experiments We engineer a pure state model using a single nitrogen-vacancy (NV) center in diamond at room temperature. The degeneracy of $|m_s = \pm 1\rangle$ is lifted by an external magnetic field $B=490$ G along the NV quantization axis, which also polarizes the intrinsic nitrogen nuclear spin during optical initialization. This qutrit system can be fully controlled using dual-frequency microwave pulses on-resonance with the transitions between $|m_s = 0\rangle$ and $|m_s = \pm 1\rangle$. We can thus create any
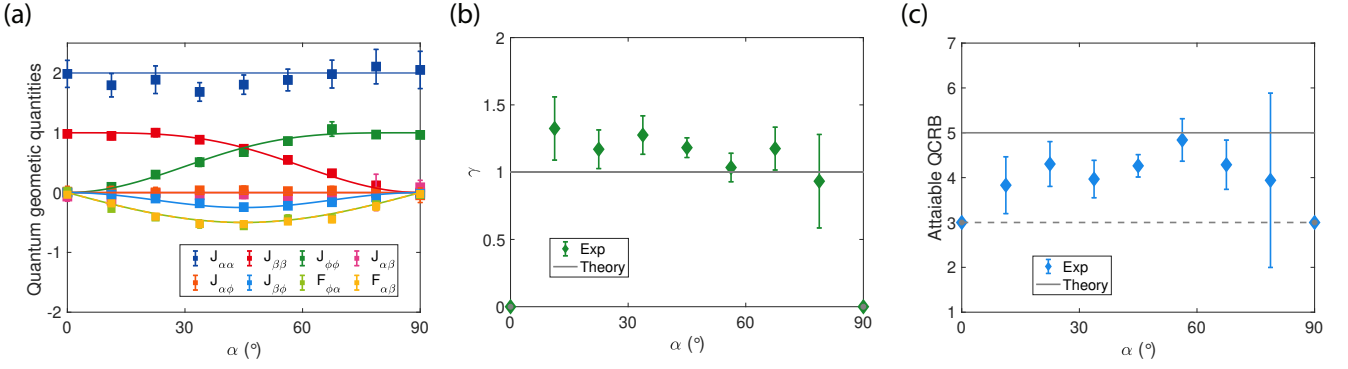
FIG. 2. **(a).** Experimental results on elements of quantum Fisher information matrix and Berry curvature matrix. The solid lines are theoretical calculations. **(b-c).** Characterization number γ (b) and corresponding attainable QCRB (c) for the three-parameter model. The solid lines are theoretical predictions in both plots. The dashed line in (c) is the attainable QCRB when $\gamma = 0$, i.e., the SLD-CRB for the model. The errorbars are propagated from the errors in quantum geometric quantities. We note that the measured γ values can deviate from or even be above one when $\alpha \in (0, \pi/2)$ and this is due to the fact that the geometric quantities are measured in separate experiments.

state parametrized by three angles,

$$|\psi(\alpha, \beta, \phi)\rangle = \frac{1}{\sqrt{2}} \begin{pmatrix} \cos(\alpha)e^{-i\beta} \\ -1 \\ \sin(\alpha)e^{-i\phi} \end{pmatrix}. \quad (11)$$

We measure the QGT of the this state to determine the QFIM and Berry curvature matrix to characterize both its geometry and multi-parameter estimation properties. Specifically, we measure all the components of the real and imaginary part of the QGT separately using weak modulations of the parameters $\mu, \nu \in \{\alpha, \beta, \phi\}$, a method that has been explored in previous work [29–31]. While more details can be found in ref [29], here we briefly illustrate the principles of the measurement.

To extract the real part of the QGT, we first prepare the state in Eq. (11) with a two-tone microwave pulse after initialization to $|m_s = 0\rangle$. We then apply driving with in-phase modulation of the amplitudes μ, ν, i.e., $\mu(t) = \mu_0 + m_\mu \sin(\omega t)$ and $\nu(t) = \nu_0 + m_\nu \sin(\omega t)$ with $|m_\mu|, |m_\nu| \ll 1$. Similarly, the imaginary part of the QGT can be extracted with out-of-phase modulations, where $\mu(t) = \mu_0 + m_\mu \sin(\omega t)$ and $\nu(t) = \nu_0 + m_\nu \cos(\omega t)$. These weak periodic modulations of the parameters will drive Rabi oscillations between the state in Eq. (11) and the other two eigenstates of the qutrit system, when the driving frequency ω is on-resonance with the energy splitting between $|\psi(\alpha, \beta, \phi)\rangle$ and the other two eigenstates $|\psi_1\rangle = (-\sin\alpha e^{-i\beta}, 0, \cos\alpha e^{-i\phi})^T$ and $|\psi_2\rangle = (\cos\alpha e^{-i\beta}, 1, \sin\alpha e^{-i\phi})^T$. Following the technique introduced in Ref. [29], we can extract the QGT, and thus the QFIM, by measuring the resulting Rabi frequencies [23].

The QGT components reconstructed using this technique are shown in Fig. 2(a). The measurement results are in good agreement with the theoretical predictions

derived from the definition of quantum geometry tensor,

$$\boldsymbol{J}(\alpha, \beta, \phi) = \begin{pmatrix} 2 & 0 & 0 \\ 0 & 2\cos^2(\alpha) - \cos^4(\alpha) & -\frac{1}{4}\sin^2(2\alpha) \\ 0 & -\frac{1}{4}\sin^2(2\alpha) & 2\sin^2(\alpha) - \sin^4(\alpha) \end{pmatrix} \quad (12)$$

and

$$\boldsymbol{F}(\alpha, \beta, \phi) = \frac{1}{2} \begin{pmatrix} 0 & \sin(2\alpha) & -\sin(2\alpha) \\ -\sin(2\alpha) & 0 & 0 \\ \sin(2\alpha) & 0 & 0 \end{pmatrix}. \quad (13)$$

The characterization number γ can then be determined as in Fig. 2(b). When $\alpha = 0$ or $\frac{\pi}{2}$, the parameterized model Eq. 11 effectively becomes a qubit system in a one-parameter (sub)space. For example, when $\alpha = 0$ we have $J_{\phi\phi} = 0$, meaning that we have no information on ϕ, and $\boldsymbol{F} = 0$, indicating that there are no non-commuting generators, and the parameter β can be estimated trivially. The model is thus quasi-classical. When $\alpha \in (0, \frac{\pi}{2})$, however, the model is coherent with $\gamma = 1$, indicating the maximal non-commutativity of the generators corresponding to the three parameters.

We can further measure the attainable QCRB, Fig. 2(c). Again, when $\alpha = 0$ or $\frac{\pi}{2}$, the attainable QCRB is equal to the SLD-CRB and HCRB, i.e., $C = C^S = C^H$ due to the quasi-classical nature of the system. In all other cases, when $\gamma = 1$, the attainable QCRB is equal to the HCRB [22] and is higher than SLD-CRB due to the incompatibility of the three parameters. From a geometric point of view, this three-level model corresponds to the ground state of a 4D Weyl-type Hamiltonian in spherical coordinates, that hosts a tensor monopole at the origin [29]. We can rewrite the characterization num-
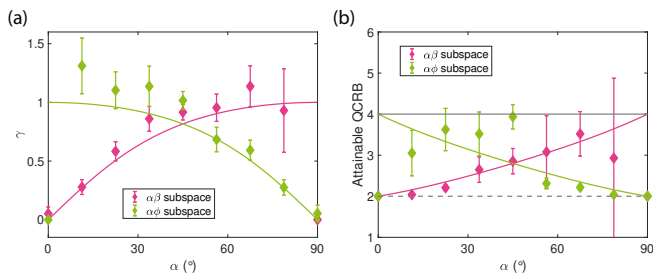
FIG. 3. . Characterization number **(a)** and attainable QCRB **(b)** for two-parameter estimation in the subspace of three-parameter model. The solid colored lines are theoretical calculations in both figures. At $\alpha = 0(\pi/2)$, the predicted value for γ (attainable QCRB) is 0 (2). The solid (dashed) black lines in (b) are attainable QCRB values when $\gamma = 1$ ($\gamma = 0$).

ber as

$$\gamma = 2\frac{\sqrt{J_{\phi\phi}F_{\alpha\beta}^2 + J_{\beta\beta}F_{\alpha\phi}^2 - 2J_{\beta\phi}F_{\alpha\beta}F_{\alpha\phi}}}{\sqrt{\det \boldsymbol{J}}} \equiv \frac{2\mathcal{H}_{\alpha\beta\phi}}{\sqrt{\det \boldsymbol{J}}}. \tag{14}$$

When $\gamma = 1$, one recovers the relation between the generalized 3-from curvature $\mathcal{H}$ and metric tensor $\boldsymbol{g}$, $\mathcal{H} = \frac{1}{2}\sqrt{\det \boldsymbol{J}} = 4\sqrt{\det \boldsymbol{g}}$. The integral of the curvature over the S^3 sphere yields the Dixmier-Douady invariant, which is the topological number for a tensor monopole and its related Kalb-Ramond field [28, 29].

The above three-parameter model enables us to study both quasi-classical ($\gamma = 0$) and coherent ($\gamma = 1$) cases. That model, as well as the two-level model $|\psi(\theta, \phi)\rangle = \cos\left(\frac{\theta}{2}\right)|0\rangle - \sin\left(\frac{\theta}{2}\right)e^{-i\phi}|1\rangle$, is indeed one of the eigenstates of a gapless Weyl-type Hamiltonian that hosts monopoles at the origin of parameter space [27, 29], leading to $\gamma = 1$ (or 0 at special points). To study intermediate cases where $\gamma \leq 1$, one can consider different geometrical models [32] or, as done here, rely on the two-parameter subspaces of the above three-parameter model where γ is a function of α. From the viewpoint of the Hamiltonian, this corresponds to taking a slice of the original gapless Weyl-type system, which yields a gapped topological insulator that can have $\gamma \leq 1$. We thus now revisit the problem of two-parameter estimation in the subspace of the qutrit system. Specifically, we focus on the subspace spanned by parameters (α, β) and (α, ϕ) (the (β, ϕ) subspace is trivial since all the corresponding Berry curvature components are zero and the SLD-CRB is attainable.) In Fig. 3 we plot the characterization number γ as well as the corresponding attainable QCRB. When $\alpha = 0(\frac{\pi}{2})$, the three-level system effectively reduces to a two-level system and the parameter $\phi(\beta)$ cannot be estimated due to the null population in $[0, 0, 1]^T$ ($[1, 0, 0]^T$). We observe γ vary continuously from 0 to 1 when sweeping α in the two subspaces. The HCRB thus ranges from 2, equal to the scalar SLD-CRB, (asymptotically) to 4, where the attainable scalar

QCRB is largest (two times larger than the SLD-CRB, as bounded by Eq. 3). These results show how γ directly predicts the attainable QCRB for subspace models, and thus sets the estimation precision when evaluating a subset of parameters. The analysis above can then be applied to scenarios where there are nuisance parameters, i.e., parameters that are not of interest but nevertheless affect the precision of estimating other parameters of interest [33–35].

While we consider a three-parameter model here, the techniques can be extended to higher dimensional models (beyond three parameters.) For example, we find that $\gamma = 1$ for the pure-state, four-parameter space model

$$|\psi(\alpha, \phi_1, \phi_2, \phi_3)\rangle = \frac{1}{\sqrt{3}}\begin{pmatrix}\cos\alpha e^{i\phi_1}\\ e^{i\phi_2}\\ \sin\alpha e^{i\phi_3}\\ 1\end{pmatrix}, \tag{15}$$

and similarly, in the subspace spanned by (α, ϕ_1, ϕ_2) and (α, ϕ_2, ϕ_3), γ varies from 0 to 1. Similar to Eq. (14), we find the relation $\gamma = 2\frac{\mathcal{E}_{\alpha\phi_1\phi_2\phi_3}}{\sqrt{\det J}} = 1$ where $\mathcal{E}_{\alpha\phi_1\phi_2\phi_3}$ is the 4-form generalized Berry curvature [23]. Its integral over the S^4 sphere will yield a topological number which is directly proportional to the second Chern number of a 5D tensor monopole [36–38].

In conclusion, we explore the relation between quantum geometry and quantum multi-parameter estimation. In addition to further insight into the ultimate precision limits, this relation enables us to experimentally extract the attainable scalar quantum Cramér-Rao bound for a three-parameter pure state model synthesized in a single spin system. We show that the SLD-CRB is not reachable due to the non-commutativity of parameter generators that affect the uncertainty relations of quantum mechanics. This bound is clarified through the link to quantum geometry, where the system properties is characterized not only the *distance* between states (the Fubini-Study metric tensor), but also by the space curvature. The present technique and discussions can provide tools and insights for finding optimal measurement strategies and evaluating the ultimate precision of multi-parameter models [17, 39–41].

* pcappell@mit.edu

[1] C. L. Degen, F. Reinhard, and P. Cappellaro, Rev. Mod. Phys. **89**, 035002 (2017).

[2] E. Marchiori, L. Ceccarelli, N. Rossi, L. Lorenzelli, C. L. Degen, and M. Poggio, Nature Reviews Physics **4**, 49 (2022).

[3] L. Thiel, Z. Wang, M. A. Tschudin, D. Rohner, I. Gutiérrez-Lezama, N. Ubrig, M. Gibertini, E. Giannini, A. F. Morpurgo, and P. Maletinsky, Science **364**, 973 (2019).

[4] K. Y. Yip, K. O. Ho, K. Y. Yu, Y. Chen, W. Zhang, S. Kasahara, Y. Mizukami, T. Shibauchi, Y. Matsuda, S. K. Goh, and S. Yang, Science **366**, 1355 (2019).

[5] M. Lesik, T. Plisson, L. Toraille, J. Renaud, F. Occelli, M. Schmidt, O. Salord, A. Delobbe, T. Debuisschert, L. Rondin, P. Loubeyre, and J.-F. Roch, Science **366**, 1359 (2019).

[6] S. Hsieh, P. Bhattacharyya, C. Zu, T. Mittiga, T. J. Smart, F. Machado, B. Kobrin, T. O. Höhn, N. Z. Rui, M. Kamrani, S. Chatterjee, S. Choi, M. Zaletel, V. V. Struzhkin, J. E. Moore, V. I. Levitas, R. Jeanloz, and N. Y. Yao, Science **366**, 1349 (2019).

[7] G. Kucsko, P. C. Maurer, N. Y. Yao, M. Kubo, H. J. Noh, P. K. Lo, H. Park, and M. D. Lukin, Nature **500**, 54 (2013).

[8] J. Choi, H. Zhou, R. Landig, H.-Y. Wu, X. Yu, S. E. V. Stetina, G. Kucsko, S. E. Mango, D. J. Needleman, A. D. T. Samuel, P. C. Maurer, H. Park, and M. D. Lukin, Proceedings of the National Academy of Sciences **117**, 14636 (2020).

[9] C. Li, R. Soleyman, M. Kohandel, and P. Cappellaro, *Nano Letters*, Nano Letters **22**, 43 (2022).

[10] A. Marais, B. Adams, A. K. Ringsmuth, M. Ferretti, J. M. Gruber, R. Hendrikx, M. Schuld, S. L. Smith, I. Sinayskiy, T. P. J. Krüger, F. Petruccione, and R. van Grondelle, Journal of The Royal Society Interface **15**, 20180640 (2018).

[11] C. Helstrom, Physics Letters A **25**, 101 (1967).

[12] H. Yuen and M. Lax, IEEE Transactions on Information Theory **19**, 740 (1973).

[13] V. P. Belavkin, Theoretical and Mathematical Physics **26**, 213 (1976).

[14] A. Holevo, Reports on Mathematical Physics **12**, 251 (1977).

[15] A. Carollo, B. Spagnolo, A. A. Dubkov, and D. Valenti, Journal of Statistical Mechanics: Theory and Experiment **2019**, 094010 (2019).

[16] J. Liu, H. Yuan, X.-M. Lu, and X. Wang, Journal of Physics A: Mathematical and Theoretical **53**, 023001 (2019).

[17] F. Albarelli, M. Barbieri, M. Genoni, and I. Gianani, Physics Letters A **384**, 126311 (2020).

[18] S. L. Braunstein and C. M. Caves, Phys. Rev. Lett. **72**, 3439 (1994).

[19] W. Guo, W. Zhong, X.-X. Jing, L.-B. Fu, and X. Wang, Phys. Rev. A **93**, 042115 (2016).

[20] M. Kolodrubetz, D. Sels, P. Mehta, and A. Polkovnikov, Physics Reports **697**, 1 (2017), geometry and non-adiabatic response in quantum and classical systems.

[21] K. Matsumoto, "Berry's phase in view of quantum estimation theory, and its intrinsic relation with the complex structure," (2000), arXiv:quant-ph/0006076.

[22] K. Matsumoto, Journal of Physics A: Mathematical and General **35**, 3111 (2002).

[23] See supplementary online material.

[24] H. P. Robertson, Phys. Rev. **46**, 794 (1934).

[25] T. Ozawa and B. Mera, Phys. Rev. B **104**, 045103 (2021).

[26] B. Mera and T. Ozawa, Phys. Rev. B **104**, 045104 (2021).

[27] B. Mera, A. Zhang, and N. Goldman, SciPost Phys. **12**, 18 (2022).

[28] G. Palumbo and N. Goldman, Phys. Rev. Lett. **121**, 170401 (2018).

[29] M. Chen, C. Li, G. Palumbo, Y.-Q. Zhu, N. Goldman, and P. Cappellaro, Science **375**, 1017 (2022).

[30] T. Ozawa and N. Goldman, Phys. Rev. B **97**, 201117 (2018).

[31] M. Yu, P. Yang, M. Gong, Q. Cao, Q. Lu, H. Liu, S. Zhang, M. B. Plenio, F. Jelezko, T. Ozawa, N. Goldman, and J. Cai, National Science Review **7**, 254 (2019).

[32] B. Mera, A. Zhang, and N. Goldman, SciPost Phys. **12**, 18 (2022).

[33] Y. Yang, G. Chiribella, and M. Hayashi, Communications in Mathematical Physics **368**, 223 (2019).

[34] J. Suzuki, Journal of Physics A: Mathematical and Theoretical **53**, 264001 (2020).

[35] J. Suzuki, Y. Yang, and M. Hayashi, Journal of Physics A: Mathematical and Theoretical **53**, 453001 (2020).

[36] C. N. Yang, *Journal of Mathematical Physics*, Journal of Mathematical Physics **19**, 320 (1978).

[37] K. Hasebe, Nuclear Physics B **886**, 952 (2014).

[38] G. Palumbo and N. Goldman, Phys. Rev. B **99**, 045154 (2019).

[39] M. Yu, Y. Liu, P. Yang, M. Gong, Q. Cao, S. Zhang, H. Liu, M. Heyl, T. Ozawa, N. Goldman, and J. Cai, "Quantum fisher information measurement and verification of the quantum cramer-rao bound in a solid-state qubit," (2020).

[40] Z. Hou, Z. Zhang, G.-Y. Xiang, C.-F. Li, G.-C. Guo, H. Chen, L. Liu, and H. Yuan, Phys. Rev. Lett. **125**, 020501 (2020).

[41] Z. Hou, J.-F. Tang, H. Chen, H. Yuan, G.-Y. Xiang, C.-F. Li, and G.-C. Guo, Science Advances **7** (2021), 10.1126/sciadv.abd2986.

Supplementary material for "A geometric perspective: experimental evaluation of the quantum Cramér-Rao bound"

Changhao Li (李长昊),[1,2] Mo Chen (陈墨),[1,3,4] and Paola Cappellaro[1,2,5,∗]

[1]*Research Laboratory of Electronics, Massachusetts Institute of Technology, Cambridge, Massachusetts 02139, USA*
[2]*Department of Nuclear Science and Engineering,*
Massachusetts Institute of Technology, Cambridge, Massachusetts 02139, USA
[3]*Institute for Quantum Information and Matter,*
California Institute of Technology, Pasadena, CA 91125, USA
[4]*Thomas J. Watson, Sr., Laboratory of Applied Physics,*
California Institute of Technology, Pasadena, CA 91125, USA
[5]*Department of Physics, Massachusetts Institute of Technology, Cambridge, Massachusetts 02139, USA*

CONTENTS

I. GENERATORS AND QUANTUM GEOMETRIC TENSOR

In this section, we introduce parameter generators discussed in main text and derive the relation between quantum geometric tensor (QGT) $\boldsymbol{\chi}$ and quantum Fisher information (QFI) $\boldsymbol{J}$. We assume a pure state model and that all operations are unitary. Instead of starting from the parametrized state such as Eq.11 in the manuscript, we begin with a probe state that is independent of the parameters to be estimated, and let it evolve to the target parametrized state through a unitary dynamics $U(\boldsymbol{\theta})$, i.e.,

$$
\begin{aligned}
|\psi(\boldsymbol{\theta})\rangle &= \exp[-iH(\boldsymbol{\theta})t]\,|\psi_0\rangle = U(\boldsymbol{\theta})\,|\psi_0\rangle \\
&\rightarrow U(\boldsymbol{\theta}+d\theta_j)\,|\psi_0\rangle = [I + (\partial_{\theta_j}U)U^\dagger d\theta_j]U\,|\psi_0\rangle \\
&= \exp\{-i[i(\partial_{\theta_j}U)U^\dagger]d\theta_j\}U\,|\psi_0\rangle\,.
\end{aligned}
\tag{S1}
$$

Here we define the generator $\mathcal{G}_\mu = i(\partial_\mu U)U^\dagger$, which describes the derivative of the unitary operator (similar as the derivative of the state vector, but in the Heisenberg picture). In this picture, all parameters to estimate influence the probe state through the unitary evolution. We can then use it to calculate the geometric quantities, as shown below.

One can apply $|\psi(\boldsymbol{\theta})\rangle \rightarrow U(\boldsymbol{\theta})\,|\psi_0\rangle$ and plug this into the definition of the QGT:

$$
\begin{aligned}
\chi_{\mu\nu} &= \langle\partial_\mu\psi|\,(I - |\psi\rangle\langle\psi|)\,|\partial_\nu\psi\rangle \\
&\rightarrow \langle\partial_\mu(U\psi_0)|\,(I - U\,|\psi_0\rangle\langle\psi_0|\,U^\dagger)\,|\partial_\nu(U\psi)\rangle \\
&= \langle\psi_0|\,\partial_\mu U^\dagger\partial_\nu U\,|\psi_0\rangle - \langle\psi_0|\,(\partial_\mu U^\dagger)U\,|\psi_0\rangle\langle\psi_0|\,(U^\dagger\partial_\nu U)\,|\psi_0\rangle
\end{aligned}
\tag{S2}
$$

The real part of $\chi_{\mu\nu}$ is given by:

$$
\begin{aligned}
g_{\mu\nu} &= \frac{1}{2}(\chi_{\mu\nu} + \chi_{\mu\nu}^\dagger) \\
&= \frac{1}{2}\,\langle\psi_0|\,(\partial_\mu U^\dagger\partial_\nu U + \partial_\nu U^\dagger\partial_\mu U)\,|\psi_0\rangle \\
&\quad + \langle\psi_0|\,(\partial_\mu U^\dagger)U\,|\psi_0\rangle\langle\psi_0|\,(\partial_\nu U^\dagger)U\,|\psi_0\rangle
\end{aligned}
\tag{S3}
$$

(it is easy to show the last term is real). Because $\mathcal{G}_\mu$ is Hermitian, $\mathcal{G}_\mu = \mathcal{G}_\mu^\dagger$, meaning $i(\partial_\mu U)U^\dagger = -iU(\partial_\mu U^\dagger)$. Using this equity, Eq. S3 becomes

$$
\begin{aligned}
g_{\mu\nu} &= \frac{1}{2}\,\langle\psi_0|\,((\partial_\mu U^\dagger)UU^\dagger\partial_\nu U + (\partial_\nu U^\dagger)UU^\dagger(\partial_\mu U))\,|\psi_0\rangle \\
&\quad - \langle\psi_0|\,(i\partial_\mu U^\dagger)U\,|\psi_0\rangle\langle\psi_0|\,(i\partial_\nu U^\dagger)U\,|\psi_0\rangle \\
&= \frac{1}{2}\,\langle\psi_0|\,\{\mathcal{G}_\mu,\mathcal{G}_\nu\}\,|\psi_0\rangle - \langle\psi_0|\,\mathcal{G}_\mu\,|\psi_0\rangle\langle\psi_0|\,\mathcal{G}_\nu\,|\psi_0\rangle \\
&= \mathrm{cov}(\mathcal{G}_\mu,\mathcal{G}_\nu) = \frac{1}{4}J_{\mu\nu}
\end{aligned}
\tag{S4}
$$

Similarly, we can find the relation between Berry curvature and the generators via

$$
\begin{aligned}
F_{\mu\nu} &= i(\chi_{\mu\nu} - \chi_{\mu\nu}^\dagger) \\
&= i\,\langle\psi_0|\,((\partial_\mu U^\dagger)UU^\dagger\partial_\nu U - (\partial_\nu U^\dagger)UU^\dagger(\partial_\mu U))\,|\psi_0\rangle \\
&= i\,\langle\psi_0|\,[\mathcal{G}_\mu,\mathcal{G}_\nu]\,|\psi_0\rangle
\end{aligned}
\tag{S5}
$$

We now reach Eq.6-7 presented in the main text.

II. MULTI-PARAMETER ESTIMATION AND UNCERTAINTY RELATIONS

In this section, we start from the well-known Heisenberg uncertainty principle and discuss its indication on the characterization number γ. While the product uncertainty relations can be extended to general multi-operator scenarios, here we consider the three-operator case and discuss its relation with γ in the three-parameter model introduced in the main text.

A. Two parameters

We start from the standard Heisenberg uncertainty relation:

$$\langle(\Delta\hat{A})^2\rangle\langle(\Delta\hat{B})^2\rangle \geq \frac{1}{4}|\langle[\hat{A},\hat{B}]\rangle|^2 \tag{S6}$$

Replace the operators $\hat{A}, \hat{B}$ with the generators of parameters μ, ν:

$$\left\langle\Delta\mathcal{G}_\mu^2\right\rangle\left\langle\Delta\mathcal{G}_\nu^2\right\rangle \geq \frac{1}{4}|\left\langle[\mathcal{G}_\mu,\mathcal{G}_\nu]\right\rangle|^2. \tag{S7}$$

From Eq. S4-S5 we get

$$J_{\mu\mu}J_{\nu\nu} \geq 4\mathcal{F}_{\mu\nu}^2. \tag{S8}$$

So the Berry curvature sets a upper bound to how precise can we estimate the parameters. Obviously, there is a trade off between estimating μ and ν (e.g. position vs momentum).

Now we consider the Robertson-Schrodinger uncertainty relation, a more stringent version of the better-known Heisenberg uncertainty relation:

$$\begin{aligned}\left\langle\Delta\hat{A}^2\right\rangle\left\langle\Delta\hat{B}^2\right\rangle &\geq \frac{1}{4}|\left\langle[\hat{A},\hat{B}]\right\rangle|^2 + \frac{1}{4}\left\langle\{\Delta\hat{A},\Delta\hat{B}\}\right\rangle^2 \\ &= \frac{1}{4}|\left\langle[\hat{A},\hat{B}]\right\rangle|^2 + Cov(\hat{A},\hat{B})^2.\end{aligned} \tag{S9}$$

Replace the operators $\hat{A}, \hat{B}$ with the generators of parameters μ, ν:

$$\left\langle\Delta\mathcal{G}_\mu^2\right\rangle\left\langle\Delta\mathcal{G}_\nu^2\right\rangle \geq \frac{1}{4}|\left\langle[\mathcal{G}_\mu,\mathcal{G}_\nu]\right\rangle|^2 + Cov(\mathcal{G}_i\mu,\mathcal{G}_\nu)^2. \tag{S10}$$

That is, $g_{\mu\mu}g_{\nu\nu} - g_{\mu\nu}^2 \geq \frac{1}{4}F_{\mu\nu}^2$, or equivalently, as stated in the main text,

$$\gamma = 2\frac{F_{\mu\nu}}{\sqrt{\det(\boldsymbol{J})}} = \frac{1}{2}\frac{F_{\mu\nu}}{\sqrt{\det(\boldsymbol{g})}} \leq 1. \tag{S11}$$

For a spin 1/2 system with state $|\psi(\theta,\phi)\rangle = \cos\frac{\theta}{2}|0\rangle - \sin\frac{\theta}{2}e^{-i\phi}|1\rangle$, one can get equality in Eq. S11, indicating that the two parameters here are informationally (maximally) exclusive.

B. Three parameters

Recall that for our spin-1 model, we have the parameterized state

$$|\psi(\alpha,\beta,\phi)\rangle = \frac{1}{\sqrt{2}}\begin{pmatrix}\cos\alpha e^{-i\beta}\\-1\\\sin\alpha e^{-i\phi}\end{pmatrix}, \tag{S12}$$

and the QGT-related matrix

$$\begin{aligned}\boldsymbol{J} = 4\boldsymbol{g} &= 4\begin{pmatrix}g_{\alpha\alpha} & g_{\alpha\beta} & g_{\alpha\phi}\\g_{\beta\alpha} & g_{\beta\beta} & g_{\beta\phi}\\g_{\phi\alpha} & g_{\phi\beta} & g_{\phi\phi}\end{pmatrix}\\ &= \begin{pmatrix}2 & 0 & 0\\0 & \cos^2\alpha(2-\cos^2\alpha) & -\frac{1}{4}\sin^2 2\alpha\\0 & -\frac{1}{4}\sin^2 2\alpha & \sin^2\alpha(2-\sin^2\alpha)\end{pmatrix}\end{aligned} \tag{S13}$$

and

$$\boldsymbol{F} = \frac{1}{2}\begin{pmatrix}0 & \sin(2\alpha) & -\sin(2\alpha)\\-\sin(2\alpha) & 0 & 0\\\sin(2\alpha) & 0 & 0\end{pmatrix}. \tag{S14}$$

We found that now we have $\gamma = 1$ for $\alpha \in (0, \frac{\pi}{2})$, as shown in the main text.

Now we can write the quantum geometric tensor in the form of parameter generators. With Eq. S4 and Eq. S5, we have

$$\langle \Delta \mathcal{G}_\alpha^2 \rangle \langle \Delta \mathcal{G}_\beta^2 \rangle \langle \Delta \mathcal{G}_\phi^2 \rangle = \langle \Delta \mathcal{G}_\alpha^2 \rangle Cov(\mathcal{G}_\beta, \mathcal{G}_\phi)^2$$
$$+ \frac{1}{4}(\langle \Delta \mathcal{G}_\phi^2 \rangle |\langle [\mathcal{G}_\alpha, \mathcal{G}_\beta] \rangle|^2 + \langle \Delta \mathcal{G}_\beta^2 \rangle |\langle [\mathcal{G}_\alpha, \mathcal{G}_\phi] \rangle|^2 + 2Cov(\mathcal{G}_\beta, \mathcal{G}_\phi)|\langle [\mathcal{G}_\alpha, \mathcal{G}_\beta] \rangle||\langle [\mathcal{G}_\alpha, \mathcal{G}_\phi] \rangle|). \tag{S15}$$

We remark that while $[\mathcal{G}_\beta, \mathcal{G}_\phi] = 0$, the parameters β and ϕ cannot be simultaneously measured with low variance since $\langle \Delta \mathcal{G}_\beta^2 \rangle \langle \Delta \mathcal{G}_\phi^2 \rangle \geq Cov(\mathcal{G}_\beta, \mathcal{G}_\phi)^2$. Indeed, these two parameters are correlated with a common parameter α and $[\mathcal{G}_\alpha, \mathcal{G}_{\beta(\phi)}] \neq 0$.

In general, for three operators $\hat{A}$, $\hat{B}$ and $\hat{C}$ that satisfies $Cov(\hat{A}, \hat{B}) = Cov(\hat{A}, \hat{C}) = 0$ and $[\hat{B}, \hat{C}] = 0$, the following equality can be deduced from $\gamma \leq 1$:

$$\langle \Delta \hat{A}^2 \rangle \langle \Delta \hat{B}^2 \rangle \langle \Delta \hat{C}^2 \rangle \geq \langle \Delta \hat{A}^2 \rangle Cov(\hat{B}, \hat{C})^2$$
$$+ \frac{1}{4}(\langle \Delta \hat{C}^2 \rangle |\langle [\hat{A}, \hat{B}] \rangle|^2 + \langle \Delta \hat{B}^2 \rangle |\langle [\hat{A}, \hat{C}] \rangle|^2 + 2Cov(\hat{B}, \hat{C})|\langle [\hat{A}, \hat{B}] \rangle||\langle [\hat{A}, \hat{C}] \rangle|). \tag{S16}$$

It's possible to have the quantum Fisher information matrix in a simple diagonal form under certain parameter transformations. The vanished off-diagonal terms then correspond to $Cov(\hat{X}, \hat{Y}) = 0$ for $\forall \hat{X}, \hat{Y} \in \{\hat{A}, \hat{B}, \hat{C}\}$. Again, from the fact that $\gamma = ||i2\boldsymbol{J}^{-1}\boldsymbol{F}||_\infty \leq 1$, we reach the generalized three-operator Heisenberg uncertainty relation

$$\langle \Delta \hat{A}^2 \rangle \langle \Delta \hat{B}^2 \rangle \langle \Delta \hat{C}^2 \rangle \geq \frac{1}{4}(\langle \Delta \hat{C}^2 \rangle |\langle [\hat{A}, \hat{B}] \rangle|^2 + \langle \Delta \hat{B}^2 \rangle |\langle [\hat{A}, \hat{C}] \rangle|^2 + \langle \Delta \hat{A}^2 \rangle |\langle [\hat{B}, \hat{C}] \rangle|^2). \tag{S17}$$

The above product inequality has also been derived by constructing positive semi-definite matrices[1–3]. The product-form uncertainty relation for N operators can be constructed in a similar manner. To this end, we showed the connection between quantum geometry with the generalized uncertainty principles.

III. QUANTUM MULTI-PARAMETER CRAMÉR-RAO BOUND

Now we show the general setting of the multi-parameter estimation problem. If the whole parameter vector is $\boldsymbol{\theta} = (\theta_0, \theta_1, \ldots, \theta_N)^T$, and the positive operator-valued measurement (POVM) set is $\{\Pi_\theta\}$, the covariance matrix of an estimator $\hat{\boldsymbol{\theta}}$ under the POVM satisfies[4]

$$\text{cov}(\hat{\boldsymbol{\theta}}, \{\Pi_\theta\}) \geq \frac{1}{n}\mathcal{I}^{-1}(\{\Pi_\theta\}) \geq \frac{1}{n}J^{-1} = \frac{1}{4n}g^{-1}, \tag{S18}$$

where $\mathcal{I}$ is the classical Fisher information, J is the QFIM, n is the repetition of the experiment, and appears naturally here as the Heisenberg scaling. The second inequality is also the (SLD) quantum Cramér-Rao bound.

The necessary and sufficient condition for the saturation of the the above SLD-CRB (the last inequality) for a pure state is to have $F_{\mu\nu} = 0$, i.e., Berry curvature is a null matrix. Since the above SLD-CRB is usually unreachable, an attainable QCRB is introduced proposed in Ref.[5,6]

$$C(\boldsymbol{\theta}) = \text{Tr}\left\{\text{Re}\left[\sqrt{\mathbb{1}_d + 2i\boldsymbol{J}(\boldsymbol{\theta})^{-1/2}\boldsymbol{F}(\boldsymbol{\theta})\boldsymbol{J}(\boldsymbol{\theta})^{-1/2}}\right]^{-2}\right\}$$
$$= \sum_i \frac{2}{1 + \sqrt{1 - |\gamma_i|^2}}, \tag{S19}$$

where $\mathbb{1}_d$ is the d-dimensional identity matrix and γ_i is the i-th eigenvalue of $i2\boldsymbol{J}^{-1}\boldsymbol{F}$.

The above bound coincidences with the better-known Holevo quantum Cramér-Rao bound (HCRB) when $\gamma = 0$ or 1. We note that HCRB could be at most twice as large as SLD-CRB[7]. This condition is satisfied when $\gamma = 1$ in the two-parameter model above. For the the three-parameter model discussed above, the ratio is $\frac{5}{3} < 2$.

IV. MODEL WITH FOUR PARAMETERS

As an extension of the discussed three-parameter model, we here consider the following pure state with parameters $(\alpha, \phi_1, \phi_2, \phi_3)$:

$$|\psi(\alpha, \phi_1, \phi_2, \phi_3)\rangle = \frac{1}{\sqrt{3}} \begin{pmatrix} \cos\alpha\, e^{i\phi_1} \\ e^{i\phi_2} \\ \sin\alpha\, e^{i\phi_3} \\ 1 \end{pmatrix}, \tag{S20}$$

The quantum Fisher information and Berry curvature matrices are found to be

$$
\boldsymbol{J} = 4\boldsymbol{g} = 4 \begin{pmatrix} g_{\alpha\alpha} & g_{\alpha\phi_1} & g_{\alpha\phi_2} & g_{\alpha\phi_3} \\ g_{\phi_1\alpha} & g_{\phi_1\phi_1} & g_{\phi_1\phi_2} & g_{\phi_1\phi_3} \\ g_{\phi_2\alpha} & g_{\phi_2\phi_1} & g_{\phi_2\phi_2} & g_{\phi_2\phi_3} \\ g_{\phi_3\alpha} & g_{\phi_3\phi_1} & g_{\phi_3\phi_2} & g_{\phi_3\phi_3} \end{pmatrix}
$$
$$
= \begin{pmatrix} 4/3 & 0 & 0 & 0 \\ 0 & 4/9(2\cos^2\alpha + \sin^2\alpha\cos^2\alpha) & -4/9\cos^2\alpha & -4/9\sin^2\alpha\cos^2\alpha \\ 0 & -4/9\cos^2\alpha & 8/9 & -4/9\sin^2\alpha \\ 0 & -4/9\sin^2\alpha\cos^2\alpha & -4/9\sin^2\alpha & 4/9(2\sin^2\alpha + \sin^2\alpha\cos^2\alpha) \end{pmatrix} \tag{S21}
$$

,

and

$$
\boldsymbol{F} = \frac{1}{2} \begin{pmatrix} 0 & -4/3\cos\alpha\sin\alpha & 0 & 4/3\cos\alpha\sin\alpha \\ 4/3\cos\alpha\sin\alpha & 0 & 0 & 0 \\ 0 & 0 & 0 & 0 \\ -4/3\cos\alpha\sin\alpha & 0 & 0 & 0 \end{pmatrix}. \tag{S22}
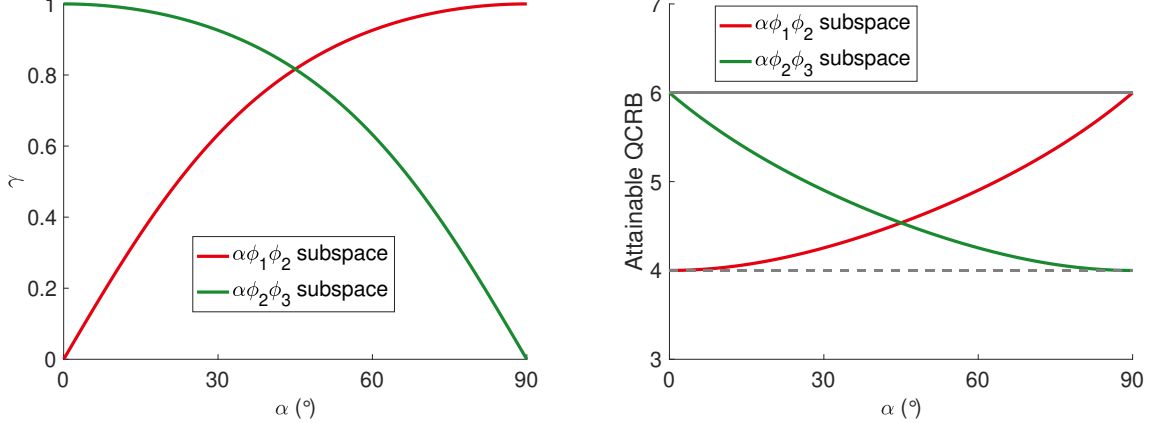$$

FIG. S1. Characterization number γ (*Left*) and attainable QCRB (*Right*) values for three-parameter subspaces in the spin $\frac{3}{2}$ model Eq. S20 for $\alpha \in (0, \pi/2)$. The solid (dashed) blacks lines in the right plot indicate the largest (=6) and smallest (=4) reachable attainable QCRB values for three-parameter models.

We note that in this model one can find an analytical expression of γ

$$\gamma = 2 \frac{\sqrt{F_{\alpha\phi_1}^2 \det(\boldsymbol{g}(\phi_2, \phi_3)) + \det(\boldsymbol{g}(\phi_1, \phi_2))F_{\alpha\phi_3}^2 - 2F_{\alpha\beta}F_{\alpha\phi}(J_{\phi_1\phi_2}J_{\phi_2\phi_3} - J_{\phi_1\phi_3}J_{\phi_2\phi_2})}}{\sqrt{\det \boldsymbol{J}}} \equiv 2\frac{\mathcal{E}_{\alpha\phi_1\phi_2\phi_3}}{\sqrt{\det \boldsymbol{J}}} \tag{S23}$$

Similarly, we find that $\gamma = 1$ for this model when $\alpha \in (0, \frac{\pi}{2})$. Here $\mathcal{E}_{\alpha\phi_1\phi_2\phi_3}$ can be regarded as the 4-form generalized Berry curvature and is related with the topological properties of the model[8–10]. The corresponding attainable QCRB for this model is $C(\boldsymbol{\theta}) = 6 > C^S(\boldsymbol{\theta}) = 4$.

Similar as the spin-1 case we discussed in the main text, we find that the $\alpha\phi_1\phi_2$ and $\alpha\phi_2\phi_3$ subspace can have varying γ values thus attainable QCRB, as shown in Fig. S1.

V. EXPERIMENT

The measurement of geometric quantities for the three-parameter model Eq. S12 is performed using the ground triplet state of a single nitrogen-vacancy (NV) center in diamond. While the details of the measurement process can be found in Ref.[11], here we give a brief introduction for the convenience of readers.

We used a home-built confocal microscope to initialize and measure a single NV center in an electronic grade diamond sample (Element 6, natural abundance of ^{13}C). A magnetic field of 490 G is applied using a permanent magnet, and the native ^{14}N nuclear spin is thus polarized and remains in $|m_I = +1\rangle$ state during the experiments due to the excited state level anti-crossing effect. The NV of interest has a long coherence time with $T_1 = 3.2$ ms and $T_{2,echo} > 700$ μs.

The target parameterized state Eq. S12 corresponds to the ground state of a 4D Weyl-type Hamiltonian,

$$H = H_0 \begin{pmatrix} 0 & \cos(\alpha)e^{-i\beta} & 0 \\ \cos(\alpha)e^{i\beta} & 0 & \sin(\alpha)e^{i\phi} \\ 0 & \sin(\alpha)e^{-i\phi} & 0 \end{pmatrix} \tag{S24}$$

To synthesis such a model, we apply dual-frequency microwave to engineer the NV system

$$
\begin{aligned}
H_{NV} =& DS_z^2 + \gamma_e B S_z \\
& + 2\sqrt{2}[\gamma_e B_1 \cos(\omega_1 t + \phi_1)S_x + \gamma_e B_2 \cos(\omega_2 t + \phi_2)]S_x
\end{aligned}
\tag{S25}
$$

where S_x, S_z are the spin-1 operators, $\gamma_e = 2.8$ MHz/G is the gyromagnetic ratio and D = 2.87 GHz is the zero-field energy splitting of the NV ground state. The first line above is the intrinsic NV spin Hamiltonian and the second line represents the dual-frequency microwave pulse at frequencies ω_1, ω_2 with amplitudes B_1, B_2 respectively. When both microwave frequencies are on-resonance $\omega_{1(2)} = D \pm \gamma_e B$, we can reach the target Hamiltonian Eq. S24 with

$$H_{NV} = \begin{pmatrix} 0 & B_1 e^{-i\phi_1} & 0 \\ B_1 e^{i\phi_1} & 0 & B_2 e^{i\phi_2} \\ 0 & B_2 e^{-i\phi_2} & 0 \end{pmatrix} = H_0 \begin{pmatrix} 0 & \cos\alpha e^{-i\beta} & 0 \\ \cos\alpha e^{i\beta} & 0 & \sin\alpha e^{i\phi} \\ 0 & \sin\alpha e^{-i\phi} & 0 \end{pmatrix} \tag{S26}$$

We then apply weak periodic modulation on the parameters $\mu, \nu \in \{\alpha, \beta, \phi\}$ to measure the quantum geometric quantities[11–13]. Specifically, we consider modulations $\mu(t) = \mu_0 + m_\mu \sin(\omega t + \eta)$, $\nu(t) = \nu_0 + m_\nu \sin(\omega t)$, with $m_\mu, m_\nu \ll 1$ and the resulting Hamiltonian reads

$$H \approx H(\alpha_0, \beta_0, \phi_0) + m_\mu \partial_\mu H \sin(\omega t + \eta) + m_\nu \partial_\nu H \sin(\omega t). \tag{S27}$$

To extract the metric tensor (resp. the Berry curvature), we linearly (resp. elliptically) modulate μ, ν at $\eta = 0$ (resp. $\pi/2$). When the modulation frequency is tuned on resonance with Δ_1 (Δ_2) that is the energy gap between the state $|\psi\rangle$ in Eq. S12 and the other two eigenstates of Hamiltonian Eq. S24 $|\psi_1\rangle$ and $|\psi_2\rangle$, the parametric modulations coherently drive Rabi oscillations between $|\psi\rangle \leftrightarrow |\psi_1\rangle$ ($|\psi\rangle \leftrightarrow |\psi_2\rangle$) and the corresponding Rabi frequencies are $\Gamma_1^{\mu\nu}$ ($\Gamma_2^{\mu\nu}$). Here the superscript $\mu\nu$ means modulations on parameter μ and ν simultaneously with amplitudes $m_\mu = m_\nu$ and we will use superscript $\mu\bar{\nu}$ to denote driving with amplitudes $m_\mu = -m_\nu$.

It can be shown that the metric tensor and Berry curvature can be constructed from the Rabi frequencies

$$
\begin{aligned}
g_{\mu\mu} &= \frac{(\Gamma_1^\mu)^2}{\Delta_1^2} + \frac{(\Gamma_2^\mu)^2}{\Delta_2^2}, \\
g_{\mu\nu} &= \frac{[(\Gamma_1^{\mu\nu})^2 - (\Gamma_1^{\mu\bar{\nu}})^2]}{4\Delta_1^2} + \frac{[(\Gamma_2^{\mu\nu})^2 - (\Gamma_2^{\mu\bar{\nu}})^2]}{4\Delta_2^2} \quad \text{(linear)}, \\
F_{\mu\nu} &= \frac{[(\Gamma_1^{\mu\nu})^2 - (\Gamma_1^{\mu\bar{\nu}})^2]}{2\Delta_1^2} + \frac{[(\Gamma_2^{\mu\nu})^2 - (\Gamma_2^{\mu\bar{\nu}})^2]}{2\Delta_2^2} \quad \text{(elliptical)}.
\end{aligned}
\tag{S28}
$$

Therefore, by measuring the Rabi oscillations, we obtain the geometric quantities, as shown in Fig.2 of the main text.

---

* pcappell@mit.edu

[1] J. L. Synge, Proceedings of the Royal Society of London. A. Mathematical and Physical Sciences **325**, 151 (1971), https://royalsocietypublishing.org/doi/pdf/10.1098/rspa.1971.0162.

[2] H.-H. Qin, S.-M. Fei, and X. Li-Jost, Scientific Reports **6**, 31192 (2016).

[3] V. V. Dodonov, Phys. Rev. A **97**, 022105 (2018).

[4] J. Liu, H. Yuan, X.-M. Lu, and X. Wang, Journal of Physics A: Mathematical and Theoretical **53**, 023001 (2019).

[5] K. Matsumoto, "Berry's phase in view of quantum estimation theory, and its intrinsic relation with the complex structure," (2000), arXiv:quant-ph/0006076.

[6] K. Matsumoto, Journal of Physics A: Mathematical and General **35**, 3111 (2002).

[7] A. Carollo, B. Spagnolo, A. A. Dubkov, and D. Valenti, Journal of Statistical Mechanics: Theory and Experiment **2019**, 094010 (2019).

[8] C. N. Yang, *Journal of Mathematical Physics*, Journal of Mathematical Physics **19**, 320 (1978).

[9] K. Hasebe, Nuclear Physics B **886**, 952 (2014).

[10] G. Palumbo and N. Goldman, Phys. Rev. B **99**, 045154 (2019).

[11] M. Chen, C. Li, G. Palumbo, Y.-Q. Zhu, N. Goldman, and P. Cappellaro, Science **375**, 1017 (2022).

[12] T. Ozawa and N. Goldman, Phys. Rev. B **97**, 201117 (2018).

[13] M. Yu, P. Yang, M. Gong, Q. Cao, Q. Lu, H. Liu, S. Zhang, M. B. Plenio, F. Jelezko, T. Ozawa, N. Goldman, and J. Cai, National Science Review **7**, 254 (2019).